

The following publication Zhang, G., Wen, W., Xu, B., & Hsu, L. T. (2020). Extending shadow matching to tightly-coupled GNSS/INS integration system. IEEE Transactions on Vehicular Technology, 69(5), 4979-4991 is available at <https://doi.org/10.1109/TVT.2020.2981093>

# Extending Shadow Matching to Tightly-coupled GNSS/INS Integration System

Guohao Zhang, Weisong Wen, Bing Xu, Li-Ta Hsu, *Member, IEEE*

**Abstract**—Performing precise positioning is still challenging for autonomous driving. Global navigation satellite system (GNSS) performance can be significantly degraded due to the non-line-of-sight (NLOS) reception. Recently, the studies of 3D building model aided (3DMA) GNSS positioning show promising positioning improvements in urban canyons. In this study, the benefits of 3DMA GNSS are further extended to the GNSS/inertial navigation system (INS) integration system. Based on the shadow matching solution and scoring information of candidate positions, two methods are proposed to better classify the line-of-sight (LOS) and NLOS satellite measurements. Aided by the satellite visibility information, the NLOS-induced pseudorange measurement error can be mitigated before fusing GNSS with the INS in the loosely-coupled or tightly-coupled integration system. Both the proposed satellite visibility estimation methods achieve over 80% LOS/NLOS classification accuracy for most of the scenarios in the urban area, which are at least 10% improvement over the carrier-to-noise ratio ( $C/N_0$ )-based method. By further extending the satellite visibility estimation to exclude NLOS measurements and adjust the measurement noise covariance, the proposed 3DMA GNSS/INS tightly-coupled integrated positioning achieves nearly a factor of 3 improvements comparing to the conventional GNSS/INS integration method during the vehicular experiment in the urban canyon.

**Index Terms**—GNSS, sensor integration, localization, 3D building model

## I. INTRODUCTION

Autonomous driving has been rapidly developed in recent years, aiming to contribute the intelligent transportation system with better safety [1] and efficiency [2]. Precise positioning is one of the fundamental requirements for autonomous vehicle [3], [4]. To improve the positioning accuracy, various kinds of sensors are employed, referred to as integrated navigation systems. A conventional approach is the global navigation satellite system/inertial navigation system (GNSS/INS) integration by a Kalman filter [5]–[7]. Using the prior-knowledge, system noise covariance and/or measurement noise covariance can be adaptively tuned, namely the adaptive Kalman filter (AKF) integration [8], [9]. Using GNSS carrier measurements and corrections from the base station, real-time

kinematic (RTK) positioning provides centimeter-level accuracy in open-sky areas [10]. Vision sensors can also be integrated into the multi-sensor system for localization [11], [12]. With the increasing computing power, light detection and ranging (LiDAR) sensors are widely used to perform accurate positioning by applying the simultaneous localization and mapping (SLAM) technique [13], [14]. Although various sensors can provide accurate positioning solutions, GNSS is still the most commonly used approach due to its advantages on low cost, global coverage and all-weather functionality, etc.

However, GNSS positioning performance can be highly degraded in dense urban areas [15], where signals can easily be blocked or reflected by buildings, vehicles, and other obstacles, causing the multipath effect or non-light-of-sight (NLOS) reception [16]. The reflected signal travels an extra distance, which finally causes a mean positioning error exceeding 40 meters [17]. Besides employing additional sensors, many efforts have been made to recover the standalone GNSS performance in a challenging environment. A straight-forward method is to adjust the weighting of each GNSS measurement during positioning based on satellite elevation and carrier-to-noise ratio ( $C/N_0$ ), namely the weighted least square (WLS) positioning method [18]. Unfortunately, the reflected signal could have a higher  $C/N_0$  than that of the line-of-sight (LOS) signal, resulting in an erroneous weighting. Another method is the consistency-check of GNSS pseudorange measurements [19], [20]. However, the measurements may contain multiple outliers in a harsh environment, forming another consistency pattern and hard to be detected. Based on the features extracted from GNSS measurements, the machine learning algorithm can be employed to classify multipath or NLOS reception signals [21]. Based on its classification, multipath and NLOS reception can be excluded to achieve better positioning accuracy. However, the classification accuracy by machine learning is environmentally depending, which is hard to maintain good performance for different scenarios. With the development of GNSS antennas, the multipath effect can be significantly mitigated by the antenna array [22]. However, the complex-designed antenna is required for this method.

Since GNSS signal reflection is mainly caused by the building surface, recent researches propose to utilize the 3D

This paragraph of the first footnote will contain the date on which you submitted your paper for review. This research was supported by the fund of “Fundamental Research on Free Exploration Category of Shenzhen Municipal Science and Technology Innovation Committee (Project No. JCYJ20170818103653507)”.

Guohao Zhang, Bing Xu and Li-Ta Hsu are with the Interdisciplinary Division of Aeronautical and Aviation Engineering, The Hong Kong Polytechnic University, Hong Kong (e-mail: lt.hsu@polyu.edu.hk)

Weisong Wen is with the Department of Mechanical Engineering, The Hong Kong Polytechnic University, Hong Kong

building model to improve positioning accuracy in urban areas, which is referred to as 3D mapping aided (3DMA) GNSS positioning. One of the well-known 3DMA GNSS positioning methods is shadow matching [23], [24]. By searching for a candidate position with the measured satellite visibility best matching the predicted satellite visibility, the user position is determined without using pseudorange measurements. On the other hand, the 3DMA GNSS likelihood-based ranging is developed to integrate the 3D building model with the GNSS measurement in a different way [25]. By comparing the differential pseudorange measurement with the differential true range, the measurement likelihood between truth can be estimated for each candidate position. By further complementarily integrating the shadow matching and the 3DMA likelihood ranging, an accurate positioning solution can be obtained in urban scenario [26]. Another approach, based on the 3D building model, the reflected GNSS signal can be simulated using the ray-tracing algorithm [27]. Therefore, the user position can be better determined by matching the measurement with the simulated reflection-included pseudorange measurements [28]-[30]. Since the ray-tracing method simulates the pseudorange measurement from each of the involving building surfaces, computational load is heavy for real-time applications. Different approaches have been proposed to reduce the computational load for more practical implementations [31], [32].

Although the 3DMA GNSS algorithm is able to obtain a promising improvement in positioning accuracy, its standalone performance is still insufficient for autonomous driving applications. The multi-sensor integration aims to achieve lane-level accuracy. It is well-deserved to further fuse the 3DMA GNSS solutions into conventional integration system. However, the 3DMA GNSS solution is usually conducted in the position domain, which limits its use only for the loosely-coupled integration [33]. In [34], the shadow matching solution is used to select GNSS pseudorange rate measurements for a velocity filter. In this study, the idea of shadow matching is extended to aid the GNSS/INS integrated positioning for the urban scenario application. By using the shadow matching estimated satellite visibility to select healthy measurements, the enormous NLOS error can be mitigated for the GNSS/INS integrated positioning. The satellite visibility is also used to

adjust the measurement noise covariance in the sensor integration. Hence, the overall positioning accuracy is improved from 22.6 meters (standalone GNSS solution) and 18.9 meters (conventional GNSS/INS tightly-coupled solution) to 6.5 meters in root mean square error (RMSE). The contributions of this study are twofold: 1) the proposed algorithm provides an accurate satellite visibility estimation, with at least 10% improvement over the conventional  $C/N_0$  based method for most cases; 2) the proposed algorithm extends the benefits of the 3DMA GNSS to exclude NLOS measurements and adaptively tune the measurement noise covariance, in order to improve the tightly-coupled GNSS/INS integrated positioning performance.

The paper is structured as following: The overview of the proposed algorithm will be introduced in Section 2. The methodology of the 3DMA GNSS shadow matching positioning will be briefly explained in Section 3. The loosely-coupled and tightly-coupled GNSS/INS integration architecture will be introduced in Section 4. The methodology of the proposed shadow matching aided GNSS/INS integrated positioning will be elaborated in Section 5. In Section 6, the performance of the proposed algorithm is verified with several experiments including vehicular tests. Finally, the conclusions are drawn in Section 7.

## II. OVERVIEW OF THE PROPOSED ALGORITHM

Then, the satellite visibility can be estimated from the shadow matching-estimated position with the surrounding building model, which is called the solution-based approach in this paper. The satellite visibility can also be estimated by the visibility and score information on each candidate position in the process of shadow matching positioning, which is referred to as the grid-based method in this paper. On the other hand, the inertial measurement unit (IMU)

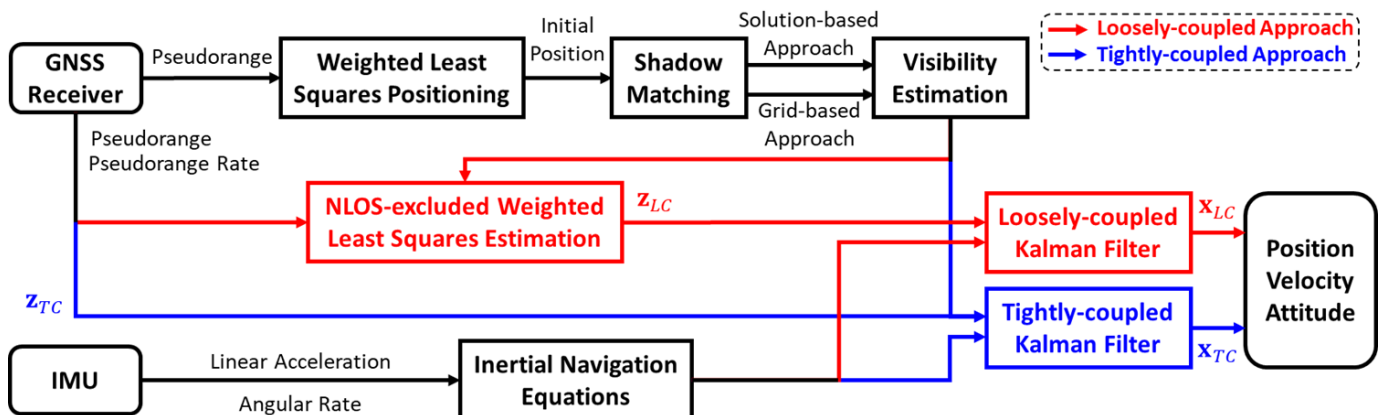


Fig. 1. The flowchart of the proposed shadow matching aided GNSS/INS integrated positioning system.

measures the linear acceleration and the angular rate of the user, which are further applied with inertial navigation equations to predict the user’s position, velocity and attitude. For the loosely-coupled approach, the estimated satellite visibility is employed to exclude the GNSS NLOS measurements, including pseudorange and pseudorange rate (computed from the Doppler frequency). After that, the NLOS-excluded GNSS measurements are applied with weighted least squares to estimate the user position and velocity, which are further integrated with the INS estimation to obtain the final position, velocity and attitude estimation. For the tightly-coupled approach, the GNSS measurements aided with the visibility information are directly integrated with the INS estimation by a Kalman filter to estimate the final user position, velocity and attitude solution.

### III. 3DMA GNSS SHADOW MATCHING

GNSS pseudorange measurements are usually containing enormous errors in urban areas due to the signal reflections. By combining building model information with the GNSS measurement availability, the shadow matching estimates the user position without using the inaccurate pseudorange measurements. Various studies have shown its feasibility and remarkable performance in urban positioning [35]. In this study, the methodology of the shadow matching positioning is based on [26].

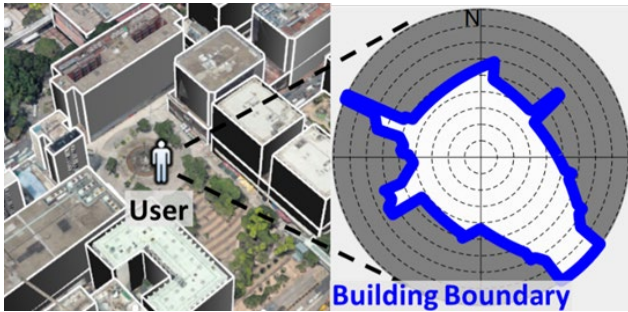


Fig. 2. The skymask of a user location, illustrated by the building boundary (in blue) with the elevation at each azimuth. The grey area denotes the areas where the sky-view is blocked by buildings.

The shadow matching determines the user’s position by searching the candidate positions with the satellite visibility that is most consistent with the actual measurements. Firstly, a certain area around the conventional GNSS solution is uniformly divided into several grids, denoting different candidate positions. The relative elevation and azimuth angle between the building edge and a specific grid location can be derived based on the surrounding 3D building model. By scanning all the azimuth angles (0-360 degrees), we can construct the building boundary in a polar coordinate system, as the blue curve in Fig. 2. Therefore, the sky-view blockage corresponding to each grid can be described with the grey area below the building boundary elevations, namely the skymask. Based on the skymask and the satellite position from the ephemeris, satellite visibility can be predicted in a probability domain for each grid as  $P_{n,skym}^i$  [26]. On the other hand, the satellite visibility can also be estimated by whether the GNSS

signal can be received in the measurement. Since the reflected NLOS signal in measurements may lead to an incorrect visibility estimation, a carrier-to-noise ratio ( $C/N_0$ ) based model [26] is used to estimate the satellite visible probability from the measurements, as  $P_{n,cnr}^i$ . By further comparing the measurement-estimated visibility with the skymask-predicted visibility of a specific grid, the probability that a satellite has the same visibility status can be computed as below, denoted as  $P_{n,match}^i$  for the  $i^{th}$  satellite on the  $n^{th}$  grid.

$$P_{n,match}^i = P_{n,skym}^i P_{n,cnr}^i + (1 - P_{n,skym}^i)(1 - P_{n,cnr}^i) \quad (1)$$

Finally, the user position is determined by weighted averaging all the grid positions based on their corresponding visibility similarity score [26], as below

$$\Lambda_n = \prod_i P_{n,match}^i / \sum_n \prod_i P_{n,match}^i \quad (2)$$

$$\hat{\mathbf{s}}_{SDM} = \sum_n \Lambda_n \mathbf{s}_n \quad (3)$$

where  $\Lambda_n$  is the normalized visibility similarity score,  $\mathbf{s}_n$  is the position of the  $n^{th}$  grid and  $\hat{\mathbf{s}}_{SDM}$  is the estimated user position.

### IV. GNSS/INS INTEGRATION

The GNSS is capable to estimate the absolute position of a user without accumulated error. On the other hand, the INS is a self-contained system providing positioning solutions with a high sampling rate. By complementarily integrating the GNSS and INS, a more accurate and reliable positioning solution can be obtained. The majority of the GNSS/INS integration methods are employing loosely-coupled or tightly-coupled architecture.

#### A. Loosely-coupled GNSS/INS Integration

The loosely-coupled (LC) GNSS/INS integrated positioning fuses the GNSS position-domain solution with the INS estimations through a Kalman filter. In this study, a basic loosely-coupled GNSS/INS integration system is implemented in the earth-centered earth-fixed (ECEF) frame as introduced in [5]. The state vector of the loosely-coupled integration is as follows

$$\mathbf{x}_{LC} = [\delta\boldsymbol{\theta}^T, \delta\boldsymbol{v}^T, \delta\mathbf{s}^T, \mathbf{b}_a^T, \mathbf{b}_g^T]^T \quad (4)$$

where  $\delta\boldsymbol{\theta}$ ,  $\delta\boldsymbol{v}$  and  $\delta\mathbf{s}$  denote the attitude, velocity and position error vector, respectively.  $\mathbf{b}_a$  denotes the accelerometer bias and  $\mathbf{b}_g$  denotes the gyroscope bias. The transition matrix  $\mathbf{F}$  is formed with first-order approximation as below

$$\mathbf{F}_{LC} = \begin{bmatrix} \mathbf{I}_3 - \boldsymbol{\omega}\tau & \mathbf{0}_3 & \mathbf{0}_3 & \mathbf{0}_3 & \mathbf{C}_b^e \tau \\ \mathbf{F}_{21} & \mathbf{I}_3 - 2\boldsymbol{\omega}\tau & \mathbf{F}_{23} & \mathbf{C}_b^e \tau & \mathbf{0}_3 \\ \mathbf{0}_3 & \mathbf{I}_3 \tau & \mathbf{I}_3 & \mathbf{0}_3 & \mathbf{0}_3 \\ \mathbf{0}_3 & \mathbf{0}_3 & \mathbf{0}_3 & \mathbf{I}_3 & \mathbf{0}_3 \\ \mathbf{0}_3 & \mathbf{0}_3 & \mathbf{0}_3 & \mathbf{0}_3 & \mathbf{I}_3 \end{bmatrix} \quad (5)$$

where  $\mathbf{I}_3$  denotes a 3-by-3 identity matrix,  $\boldsymbol{\omega}$  is the symmetric

matrix of earth rate,  $\tau$  is the propagation interval,  $\mathbf{C}_b^e$  is the coordinate transformation matrix from the body frame to ECEF frame.  $\mathbf{F}_{21}$  denotes the velocity error term due to the attitude.  $\mathbf{F}_{23}$  denotes the velocity error term due to the gravity. The measurement model matrix  $\mathbf{H}_{LC}$  and the measurement vector  $\mathbf{z}_{LC}$  are as follows

$$\mathbf{H}_{LC} = \begin{bmatrix} \mathbf{0}_3 & \mathbf{0}_3 & -\mathbf{I}_3 & \mathbf{0}_3 & \mathbf{0}_3 \\ \mathbf{0}_3 & -\mathbf{I}_3 & \mathbf{0}_3 & \mathbf{0}_3 & \mathbf{0}_3 \end{bmatrix} \quad (6)$$

$$\mathbf{z}_{LC} = [\mathbf{s}_{GNSS}^T, \mathbf{v}_{GNSS}^T]^T \quad (7)$$

Where  $\mathbf{s}_{GNSS}$  and  $\mathbf{v}_{GNSS}$  denote the position and velocity solutions from the GNSS respectively. The system noise covariance matrix  $\mathbf{Q}_{LC}$  and the measurement noise covariance matrix  $\mathbf{R}_{LC}$  are heuristically tuned as follows

$$\mathbf{Q}_{LC} = \mathit{diag}\{\mathbf{I}_3 Q_{gn}, \mathbf{I}_3 Q_{an}, \mathbf{0}_3, \mathbf{I}_3 Q_{ab}, \mathbf{I}_3 Q_{gb}\} \quad (8)$$

$$\mathbf{R}_{LC} = \mathit{diag}\{\mathbf{I}_3 R_{pn}, \mathbf{I}_3 R_{vn}\} \quad (9)$$

Where the gyroscope noise term  $Q_{gn} = 0.005^2$  ( $rad^2$ ), the gyroscope bias term  $Q_{gb} = 4e^{-11}$  ( $rad^2/s^2$ ), the accelerometer noise term  $Q_{an} = 0.008^2$  ( $m^2/s^2$ ), the accelerometer bias term  $Q_{ab} = 1e^{-5}$  ( $m^2/s^4$ ). The GNSS position measurement noise term  $R_{pn} = 25^2$  ( $m^2$ ) and the pseudorange rate noise term  $R_{vn} = 10^2$  ( $m^2/s^2$ ). By following a standard Kalman filtering procedure, the GNSS/INS integrated solution is obtained including position, velocity and attitude.

### B. Tightly-coupled GNSS/INS Integration

Unlike the loosely-coupled integration, the tightly-coupled (TC) approach directly fuses the GNSS pseudorange and pseudorange rate with the INS estimations. Since the position-domain GNSS solution is not necessary for tightly-coupled approach, the integration can be applied without a sufficient number of satellites. Therefore, the tightly-coupled method usually achieves a more accurate and robust positioning solution, especially for the urban scenario with limited satellite visibility. Here, a basic tightly-coupled GNSS/INS integration system is implemented in the ECEF coordinate based on [5]. On the basis of the loosely-coupled approach, the state vector of the proposed tightly-coupled integration is formed with additional GNSS states, as follows

$$\mathbf{x}_{TC} = [\delta\theta^T, \delta\mathbf{v}^T, \delta\mathbf{s}^T, \mathbf{b}_a^T, \mathbf{b}_g^T, \delta\boldsymbol{\rho}_r^T, \delta\dot{\boldsymbol{\rho}}_r^T]^T \quad (10)$$

where  $\delta\boldsymbol{\rho}_r$  and  $\delta\dot{\boldsymbol{\rho}}_r$  is the receiver clock bias and drift, respectively. The number of the estimated components in  $\delta\boldsymbol{\rho}_r$  or  $\delta\dot{\boldsymbol{\rho}}_r$  is depending on the number of different constellations in use for multi-GNSS. Here, GPS and Beidou systems are employed. Hence, two receiver clock biases and two clock drifts are estimated in the state vector. Similar to the loosely-coupled approach, the transition matrix  $\mathbf{F}$  with the first-order approximation is formed as follows

$$\mathbf{F}_{TC} = \begin{bmatrix} \mathbf{I}_3 - \boldsymbol{\omega}\tau & \mathbf{0}_3 & \mathbf{0}_3 & \mathbf{0}_3 & \mathbf{C}_b^e\tau & \mathbf{0}_3 & \mathbf{0}_3 \\ \mathbf{F}_{21} & \mathbf{I}_3 - 2\boldsymbol{\omega}\tau & \mathbf{F}_{23} & \mathbf{C}_b^e\tau & \mathbf{0}_3 & \mathbf{0}_3 & \mathbf{0}_3 \\ \mathbf{0}_3 & \mathbf{I}_3\tau & \mathbf{I}_3 & \mathbf{0}_3 & \mathbf{0}_3 & \mathbf{0}_3 & \mathbf{0}_3 \\ \mathbf{0}_3 & \mathbf{0}_3 & \mathbf{0}_3 & \mathbf{I}_3 & \mathbf{0}_3 & \mathbf{0}_3 & \mathbf{0}_3 \\ \mathbf{0}_3 & \mathbf{0}_3 & \mathbf{0}_3 & \mathbf{0}_3 & \mathbf{I}_3 & \mathbf{0}_3 & \mathbf{0}_3 \\ \mathbf{0}_3 & \mathbf{0}_3 & \mathbf{0}_3 & \mathbf{0}_3 & \mathbf{0}_3 & \mathbf{I}_3 & \mathbf{I}_3\tau \\ \mathbf{0}_3 & \mathbf{0}_3 & \mathbf{0}_3 & \mathbf{0}_3 & \mathbf{0}_3 & \mathbf{0}_3 & \mathbf{I}_3 \end{bmatrix} \quad (11)$$

Using the GNSS pseudorange and pseudorange rate as integration measurements, the measurement model matrix  $\mathbf{H}_{TC}$  and the measurement vector  $\mathbf{z}_{TC}$  are formed as below

$$\mathbf{H}_{TC} = \begin{bmatrix} \mathbf{0} & \mathbf{0} & \mathbf{u}^1 & \mathbf{0} & \mathbf{0} & \boldsymbol{\gamma}^1 & \mathbf{0} \\ \vdots & \vdots & \vdots & \vdots & \vdots & \vdots & \vdots \\ \mathbf{0} & \mathbf{0} & \mathbf{u}^i & \mathbf{0} & \mathbf{0} & \boldsymbol{\gamma}^i & \mathbf{0} \\ \mathbf{0} & \mathbf{u}^1 & \mathbf{0} & \mathbf{0} & \mathbf{0} & \mathbf{0} & \boldsymbol{\gamma}^1 \\ \vdots & \vdots & \vdots & \vdots & \vdots & \vdots & \vdots \\ \mathbf{0} & \mathbf{u}^i & \mathbf{0} & \mathbf{0} & \mathbf{0} & \mathbf{0} & \boldsymbol{\gamma}^i \end{bmatrix} \quad (12)$$

$$\mathbf{z}_{TC} = [\rho^1 \quad \dots \quad \rho^i \quad \dot{\rho}^1 \quad \dots \quad \dot{\rho}^i]^T \quad (13)$$

where  $\mathbf{u}^i$ ,  $\rho^i$  and  $\dot{\rho}^i$  are the unit line-of-sight vector, pseudorange and pseudorange rate of the  $i^{th}$  satellite, respectively. For the  $i^{th}$  satellite belongs to the  $k^{th}$  constellation,  $\boldsymbol{\gamma}^i$  is the indicator of constellation having value 1 on the  $k^{th}$  column and 0 on others. The system noise covariance matrix  $\mathbf{Q}_{TC}$  and the measurement noise covariance matrix  $\mathbf{R}_{TC}$  are formed with additional terms comparing to the loosely-coupled approach, as follows

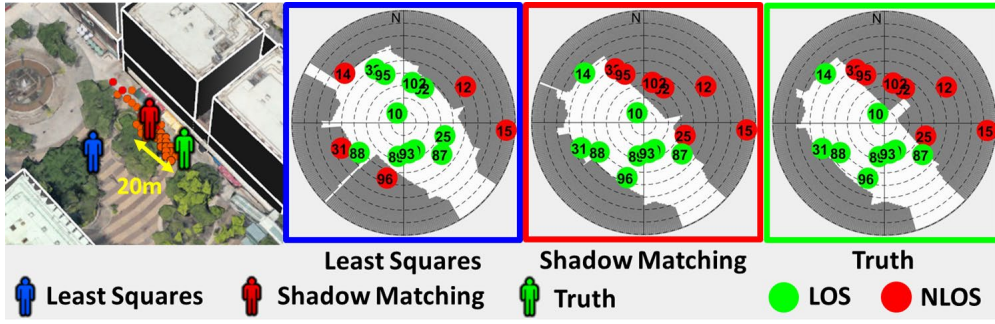
$$\mathbf{Q}_{TC} = \mathit{diag}\{\mathbf{I}_3 Q_{gn}, \mathbf{I}_3 Q_{an}, \mathbf{0}_3, \mathbf{I}_3 Q_{ab}, \mathbf{I}_3 Q_{gb}, \mathbf{I}_3 Q_{cfd}, \mathbf{I}_3 Q_{cpd}\} \quad (14)$$

$$\mathbf{R}_{TC} = \mathit{diag}\{\mathbf{I}_I R_{prn}, \mathbf{I}_I R_{prrn}\} \quad (15)$$

The receiver clock frequency drift term  $Q_{cfd} = 1$  ( $m^2/s^2$ ) and the receiver clock phase drift term  $Q_{cpd} = 1$  ( $m^2$ ).  $\mathbf{I}_I$  denotes an  $I$ -by- $I$  identity matrix where  $I$  is the total amount of the satellite providing measurements. The pseudorange noise term  $R_{prn} = 50^2$  ( $m^2$ ) and the pseudorange rate noise term  $R_{prrn} = 25^2$  ( $m^2/s^2$ ). Following a basic Kalman filtering procedure, the user position, velocity and attitude can be estimated.

### V. SHADOW MATCHING AIDED GNSS/INS INTEGRATION

In urban areas, the reflected GNSS NLOS signal is very likely to be received by the receiver, resulting in enormous errors in the pseudorange measurements, which is challenging even for the GNSS/INS system. On one hand, the INS is hard to provide long-term accurate stand-alone solutions due to its accumulated error, especially for those low-cost sensors in civil applications. On the other hand, the NLOS reception can be continuously received, which means the GNSS performance will be continuously degraded. To solve this problem, a common approach is to detect and exclude the NLOS measurements prior to integration.



### A. Shadow Matching Solution-based Satellite Visibility

To distinguish the NLOS measurements from the received measurements, a straight-forward method is to compare the position of the received satellites with the skymask on the receiver's location. However, it is not applicable because the true location of the receiver is unknown. As Fig. 3 shows, due to a large positioning error, the satellite visibility based on the conventional least squares (LS) solution is very different from the truth (GT). Since the shadow matching is determining the position by matching the satellite visibility, the solution is more likely to have similar visibility to that at the truth. Even though the shadow matching solution may contain a certain error, the corresponding satellite visibility is very similar to the truth.

Therefore, the receiver's satellite visibility can be estimated based on the shadow matching positioning solution and its surrounding building geometry. The LOS and NLOS satellites are classified by Algorithm 1. The skymask database stores each candidate position's skymask information. Based on the skymask of the shadow matching solution, the building boundary elevation corresponding to each satellite's azimuth can be obtained. If the satellite elevation is lower than its corresponding building boundary elevation, this satellite is classified as NLOS. Otherwise, it is classified as LOS. By using the LOS-classified measurement only, the enormous NLOS error can be mitigated, guaranteeing the performance of GNSS/INS integrated positioning.

---

#### Algorithm 1 Shadow Matching Solution-based Satellite Visibility Estimation

---

**Input:** Shadow matching positioning solution  $\mathbf{s}_{shadow\ matching}$ , skymask database, satellite elevations  $\mathbf{El} = \{El^1, El^2, \dots, El^I\}$  and azimuths  $\mathbf{Az} = \{Az^1, Az^2, \dots, Az^I\}$

**Output:** LOS satellite set  $I_{LOS}$ , NLOS satellite set  $I_{NLOS}$

- 1 Obtain the building boundary elevations  $El_{building}$  corresponding to  $\mathbf{s}_{shadow\ matching}$  from the skymask database
  - 2 **for**  $i = 1 \rightarrow I$  **do**
  - 3   obtain the satellite elevation  $El^i \in \mathbf{El}$  and azimuth  $Az^i \in \mathbf{Az}$
  - 4   obtain the building boundary elevation  $El_{building}(Az^i)$  on azimuth  $Az^i$
  - 5   **if**  $El^i > El_{building}(Az^i)$
  - 6     add  $i$  into the satellite set  $I_{LOS}$
  - 7   **else**
  - 8     add  $i$  into the satellite set  $I_{NLOS}$
  - 9   **end if**
  - 10 **end for**
- 

### B. Shadow Matching Grid-based Satellite Visibility

With similar skymask between different candidate positions, the shadow matching could experience a multi-modal issue

[26]. Multiple locations may highly match with the measurement-estimated visibility, even some of them are far away from each other. The final location may be misjudged by averaging the candidate positions, resulting in an incorrect visibility estimation. To mitigate this issue, a grid-based method is employed similar to [34]. Instead of directly using the final solution to estimate the visibility, the satellite visibility on each candidate position is combined by weighted averaging with the corresponding matching score. Hence, the satellite visibility can be estimated with an expression on the probability of being LOS or NLOS, which is more robust even under the multi-modal circumstance. The NLOS probability of each satellite can be estimated based on Algorithm 2. The NLOS probability of the  $i^{th}$  satellite can be estimated by

$$P_{NLOS}^i = \{\sum \Lambda_n | El_{building,n}(Az^i) > El^i\} \quad (16)$$

where  $El^i$  and  $Az^i$  are the elevation and azimuth angle of the  $i^{th}$  satellite, respectively.  $El_{building,n}(Az^i)$  is the relative building boundary elevation angle on azimuth  $Az^i$  for the  $n^{th}$  candidate. Instead of only giving a classification of being NLOS or LOS, the proposed method provides the information that how possible a satellite tends to be NLOS. Since the grid-based visibility estimation is more robust with probability information, it is more appropriate to be employed to aid the GNSS/INS integration.

---

#### Algorithm 2 Shadow Matching Grid-based Satellite Visibility Estimation

---

**Input:** Shadow matching candidate positions  $\mathbf{S} = \{\mathbf{s}_1, \mathbf{s}_2, \dots, \mathbf{s}_N\}$  and the corresponding score  $\mathbf{\Lambda} = \{\Lambda_1, \Lambda_2, \dots, \Lambda_N\}$ , skymask database, satellite elevations  $\mathbf{El} = \{El^1, El^2, \dots, El^I\}$  and azimuths  $\mathbf{Az} = \{Az^1, Az^2, \dots, Az^I\}$

**Output:** NLOS probability of each satellite  $\mathbf{P}_{NLOS} = \{P_{NLOS}^1, P_{NLOS}^2, \dots, P_{NLOS}^I\}$

- 1 **for**  $i = 1 \rightarrow I$  **do**
  - 2   obtain the satellite elevation  $El^i \in \mathbf{El}$  and azimuth  $Az^i \in \mathbf{Az}$
  - 3   **for**  $n = 1 \rightarrow N$  **do**
  - 4     obtain the building boundary elevations  $El_{building,n}$  corresponding to the  $n^{th}$  candidate position  $\mathbf{s}_n \in \mathbf{S}$  from the skymask database
  - 5     get building boundary elevation  $El_{building,n}(Az^i)$  on azimuth  $Az^i$
  - 6     **if**  $El^i < El_{building,n}(Az^i)$
  - 7        $P_{NLOS,n}^i = \Lambda_n$  where  $\Lambda_n \in \mathbf{\Lambda}$
  - 8     **else**
  - 9        $P_{NLOS,n}^i = 0$
  - 10    **end if**
  - 11   **end for**
  - 12   compute  $P_{NLOS}^i = \sum_{n=1}^N P_{NLOS,n}^i$
  - 13 **end for**
-

### C. Satellite Visibility Aided GNSS/INS Integration

In this study, the solution-based and grid-based visibility are individually employed to aid the loosely-coupled integration and the tightly-coupled integration. For the loosely-coupled approach, the LOS-classified pseudorange and pseudorange rate measurements from the solution-based method will be applied with a weighted least squares [18], in order to compute the user position and velocity [36] for fusion. For the grid-based visibility, it estimates the satellite visibility in a probability form instead of directly classifying LOS or NLOS. Therefore, similar to [34], a probability threshold is used to distinguish NLOS from all the **measurements**. The measurements with below 50% NLOS probability are classified as LOS measurements, which are similarly applied with the weighted least square to compute the GNSS position and velocity solution for integration.

For the tightly-coupled approach, the LOS-classified pseudorange and pseudorange rate measurements from the solution-based visibility estimation are directly fused with INS estimations. Since the grid-based visibility estimation provides additional operating information for the measurement from each satellite, the NLOS-probability can be further used to adaptively tune the measurement covariance matrix during integration. Firstly, the measurement with above 50% NLOS probability **is** more likely to be NLOS measurement, which will be excluded beforehand. Then, the remaining pseudorange and pseudorange rate measurements are **integrated** with INS estimation with the measurement noise covariance as following

$$R_{prn}^i = (P_{NLOS}^i \sigma_{prn,NLOS})^2 + (\sigma_{prn,LOS})^2 \quad (m^2) \quad (17)$$

$$R_{prrn}^i = (P_{NLOS}^i \sigma_{prrn,NLOS})^2 + (\sigma_{prrn,LOS})^2 \quad (m^2/s^2) \quad (18)$$

where  $\sigma_{prn,NLOS} = 120m$ ,  $\sigma_{prn,LOS} = 20m$ ,  $\sigma_{prrn,NLOS} = 40m/s$  and  $\sigma_{prrn,LOS} = 10m/s$ . Noted that the truly-LOS measurement will also experience other types of error, for example, the diffraction or multipath effect. Besides excluding NLOS measurements, the satellite visibility information can be used as the measurement reliability to adjust the measurement noise covariance matrix during GNSS/INS integration.

## VI. EXPERIMENTAL RESULTS

### A. Shadow Matching Satellite Visibility Estimation

To verify the proposed **shadow matching** satellite visibility estimation accuracy, experiments were conducted in various scenarios, including Light Urban, Middle Urban, Dense Urban, One-side Building and Intersection, as shown in Fig. 4. The red line with the arrow indicates the pedestrian trajectory. The ublox M8T Evaluate Kit was used to output the GNSS measurements for post-processing. The ground truth of this static experiment is obtained by comparing the landmark **on** Google Earth. The true satellite visibility is labeled by comparing the satellite position with the skymask of the ground truth location. **The satellite below the building boundary is NLOS, otherwise, it is LOS.**

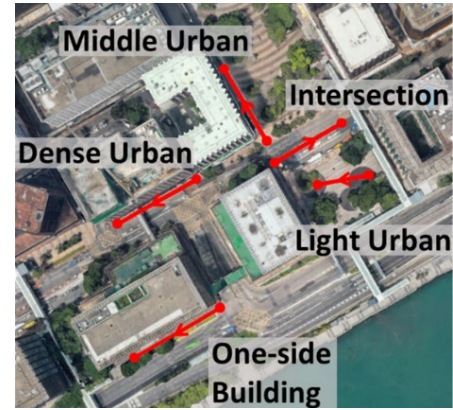


Fig. 4. The experiment routes for different scenarios in the urban area.

The accuracy of the grid-based satellite visibility estimation can be evaluated using the summation of the correctly-classified probability and normalizing it by the number of satellites. The satellite visibility can also be estimated in the form of probability using a  $C/N_0$ -based model, which is employed during shadow matching [26]. Similarly, the corresponding accuracy can be evaluated using the preceding approach. By considering the NLOS classification and LOS classification individually, the corresponding classification recall and F1 score [37] are computed respectively to evaluate the satellite visibility estimation performance.

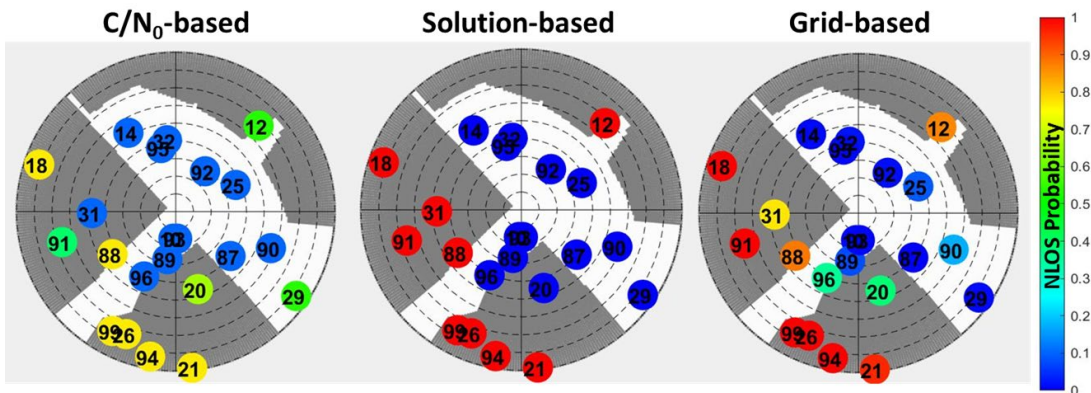


Fig. 5. The satellite visibility estimation results from the  $C/N_0$ -based method (left), the shadow matching solution-based method (middle) and the shadow matching grid-based method (right). The gray area indicates the building and the circle denotes the satellite. The color of the circle indicates the value of its NLOS probability by the color bar.

For the middle urban scenario, the satellite visibility estimations are shown in Fig. 5 for three methods, including: 1)  $C/N_0$ -based method; 2) shadow matching solution-based method and 3) shadow matching grid-based method. By using the  $C/N_0$  model, the NLOS measurements can be classified from the LOS measurements together with its probability, achieving an overall accuracy of 75.8%. However, the NLOS measurement with high  $C/N_0$  value can be misclassified to be LOS with a high probability. For the satellite-31, it is misclassified as a LOS with a probability of 90% due to its high  $C/N_0$  of 36 dB-Hz. By further adding the 3D building model information, the shadow matching solution-based method can correctly classify satellite-31 as NLOS. This method simply provides a binary result, i.e., LOS or NLOS with no probability. However, the NLOS classification rate is highly dependent on the position accuracy for this method. Unlike the solution-based methods, the grid-based solution provides the estimation with uncertainty information. For satellites that have a much lower or higher elevation angle than the building boundary at the same azimuth angle, such as satellites 91 and 92, they are classified as LOS or NLOS with high enough probability. For satellites 88 and 96 nearby the building boundary that hard to be distinguished between LOS and NLOS, the grid-based estimation remains a certain value of uncertainty instead of classifying them into pure LOS or NLOS. Even though the shadow matching solution is inaccurate, the grid-based method always gives uncertainty to tolerant fault classification based on the surrounding building information, resulting in the classification more robust and less likely being completely wrong. Rather than fully misclassifying satellite-20 as LOS by the solution-based method, the grid-based method estimates its

LOS probability as 61.6%, containing much uncertainty that it could be NLOS. Although the  $C/N_0$ -based method also estimates the satellite visibility with probability, the grid-based method further incorporates the 3D building model information for estimation. Therefore, the grid-based method has the best performance in terms of LOS/NLOS classification among the three methods.

The classification result of different methods in the middle urban scenario is shown in Fig. 6. For the availability-based method, the signal type is simply determined using the availability in the measurements, which has a bad performance in Fig. 6(top). It is interesting to note that the availability-based method has a high LOS classification rate. This is because all the available measurements are regarded as LOS, while the truly-LOS signals are always received. Whereas, the NLOS receptions are also classified as LOS. Although achieving similar overall performance, the  $C/N_0$ -based method is able to classify NLOS measurements among all available measurements by  $C/N_0$  value. Therefore, the  $C/N_0$ -based method outperforms the availability-based method for NLOS detection and exclusion. The solution-based and grid-based method achieve the classification accuracy of 94.8% and 93.7%, respectively. Both the LOS and NLOS classification rates are increased by over 15% using the two proposed methods compared to the  $C/N_0$ -based method. With a high NLOS classification rate, the NLOS-induced pseudorange measurement error is expected to be reduced. Compared to the solution-based method, the grid-based method estimates the visibility in a way of probability, thereby having a more robust performance.

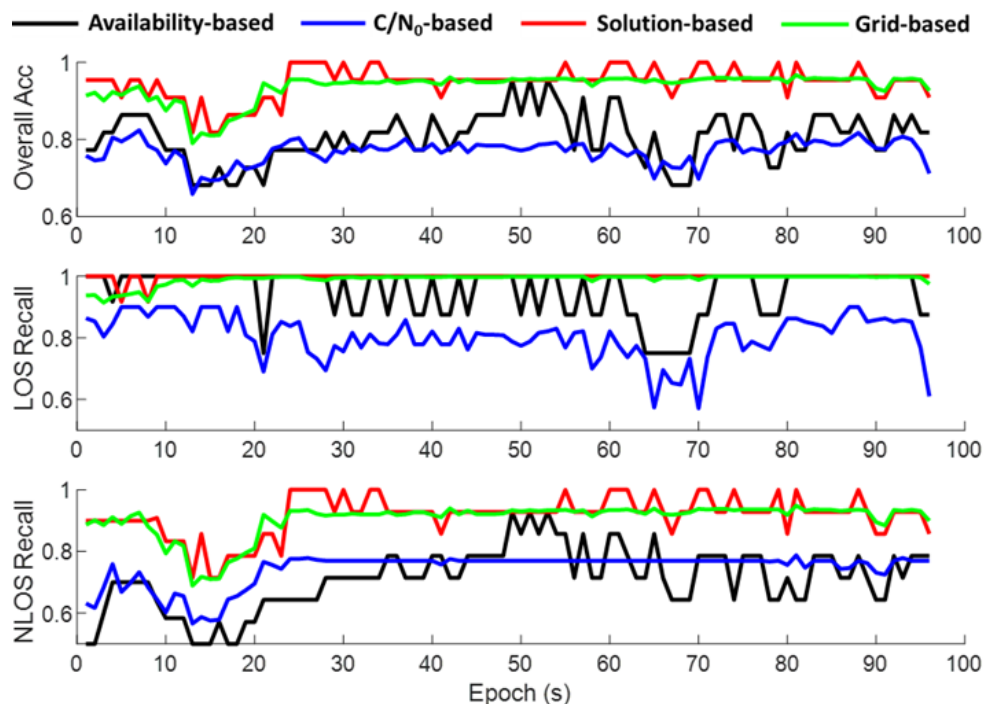


Fig. 6. The overall classification accuracy, LOS and NLOS recall from the availability-based method,  $C/N_0$ -based method, the shadow matching solution-based method and the shadow matching grid-based method for the middle urban scenario.

The satellite visibility estimation performances of the proposed methods in all scenarios are evaluated with the classification accuracy, recall and F1 score for different scenarios in Table 1. For the availability-based approach, the LOS recall is always high but the NLOS recall could be very low. Since all available measurements are regarded as the LOS measurement, this method cannot detect any NLOS in the measurements. The  $C/N_0$ -based method is more useful since it is able to detect some of the NLOS among all the received measurements. Whereas, this method only provides nearly 70% overall accuracy and lower than 70% NLOS classification recall in some scenarios. The shadow matching solution-based method is able to improve the NLOS classification recall for most cases, resulting in an overall much better performance.

However, for the scenario shadow matching not performing well, such as One-side Building, the solution-based method will be degraded. Since the proposed grid-based method is more robust with the shadow matching positioning error, it is able to maintain the NLOS classification recall with over 70% in such a difficult scenario. Compared to  $C/N_0$ -based method, the grid-based method achieves higher LOS and NLOS classification recall and nearly 10% at least improvement for the overall accuracy in all scenarios. Moreover, the proposed grid-based method always improves both the LOS and NLOS F1 score in all different scenarios, from 7.2% to 19.9%. Therefore, the shadow matching grid-based method can always better estimate the satellite visibility for different scenarios in urban.

TABLE I  
THE MEAN CLASSIFICATION ACCURACY, RECALL AND F1 SCORE OF DIFFERENT CLASSIFICATION METHODS IN THE URBAN SCENARIOS

Scenario	Classification Method	LOS		NLOS		Overall Accuracy
		Recall	F1 Score	Recall	F1 Score	
Light Urban	Availability-based	89.0%	84.7%	62.2%	67.6%	79.6%
	$C/N_0$ -based	75.3%	77.3%	66.1%	62.8%	72.3%
	Solution-based	87.8%	87.1%	75.3%	74.9%	83.4%
	Grid-based	85.6%	86.0%	76.7%	74.8%	82.7%
Middle Urban	Availability-based	95.0%	78.9%	71.2%	81.4%	80.5%
	$C/N_0$ -based	80.5%	72.4%	74.3%	79.7%	77.0%
	Solution-based	99.8%	93.8%	91.6%	95.4%	94.8%
	Grid-based	99.0%	92.5%	90.5%	94.5%	93.7%
Dense Urban	Availability-based	80.2%	60.3%	43.0%	54.5%	57.9%
	$C/N_0$ -based	71.5%	63.9%	66.0%	70.8%	67.9%
	Solution-based	64.8%	62.9%	72.2%	73.0%	68.9%
	Grid-based	73.2%	71.1%	77.6%	78.7%	75.8%
One-side Building	Availability-based	89.7%	86.7%	72.5%	76.4%	83.2%
	$C/N_0$ -based	74.5%	76.8%	70.2%	66.9%	72.9%
	Solution-based	100.0%	89.3%	61.9%	75.6%	85.2%
	Grid-based	99.1%	91.4%	71.7%	82.5%	88.5%

### B. Shadow Matching Aided GNSS/INS Integration Result



Fig. 7. Vehicular experiment route in the dense urban area (Left), and the vehicular platform (Right).

To verify the performance of the proposed shadow matching aided GNSS/INS integration method, a vehicular test was conducted. A circular testing route was selected with nearly 10 seconds GNSS-limited area operation (not enough satellite number for least squares positioning) in a dense urban area. The experiment platform is shown in Fig. 7. The GNSS measurements were collected using the Ublox M8T Evaluation Kit with a standard patch antenna. The IMU measurements

were collected by the Xsens Mti 10. The true position during the test was given by the Novatel SPAN-CPT with RTK solutions. The positioning performance is compared with the GNSS weighted least squares (WLS) positioning, conventional loosely-coupled GNSS/INS integration (LC), the shadow matching solution-based visibility aided loosely-coupled method (S-LC), the shadow matching grid-based visibility aided loosely-coupled method (G-LC), conventional tightly-coupled GNSS/INS integration (TC), the shadow matching solution-based visibility aided tightly-coupled method (S-TC), the shadow matching grid-based visibility aided tightly-coupled method (G-TC).

The overall classification accuracy and recall for the whole test period is shown in Fig. 8. Metrics of mean classification accuracy, precision, recall and F1 score are shown in Table 2. The availability-based method has an overall accuracy of 70.3%, whereas its NLOS classification recall is only 58.3%. By using the  $C/N_0$  model, the NLOS classification recall is improved to 68.6%, achieving a slightly higher overall accuracy of 72.1%. Compared to the  $C/N_0$ -based method, both the solution-based and the grid-based methods improve the NLOS recall by more than 20%, and have an overall accuracy of 90.5% and 84.8%, respectively

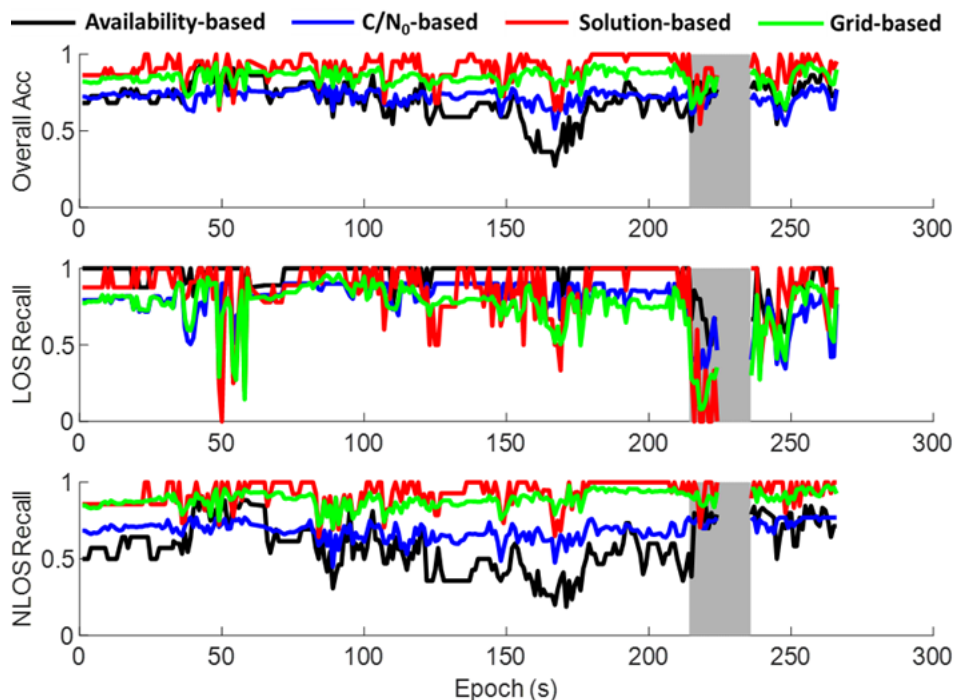


Fig. 8. The overall classification accuracy, LOS and NLOS classification recall for the availability-based method,  $C/N_0$ -based method, the shadow matching solution-based method and the shadow matching grid-based method during the vehicular test. The shaded area denotes the GNSS-limited period during the experiment.

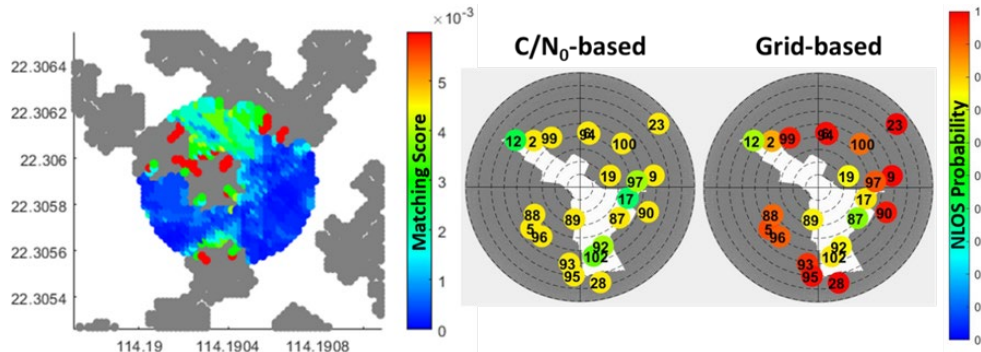


Fig. 9. Shadow matching normalized score heatmap during the epochs 211 to 231 (left) and the corresponding satellite visibility estimation results using the  $C/N_0$ -based method and the shadow matching grid-based method (right).

TABLE II

THE OVERALL PERFORMANCE OF DIFFERENT SATELLITE VISIBILITY ESTIMATION METHODS DURING THE VEHICULAR TEST							
Classification Method	Precision	LOS Recall	F1 score	Precision	NLOS Recall	F1 score	Overall Accuracy
Availability-based	53.7%	94.8%	67.1%	96.7%	58.3%	71.1%	70.3%
$C/N_0$ -based	54.3%	79.2%	63.2%	87.4%	68.6%	76.4%	72.1%
Solution-based	85.3%	83.8%	84.9%	93.6%	92.5%	92.8%	90.5%
Grid-based	74.7%	74.5%	73.8%	88.5%	88.9%	88.5%	84.8%

The environment of the vehicular test is a typical street scenario. The shadow matching performs well without the multi-modal issue during most of the testing time. Therefore, the solution-based method is slightly better than the grid-based method in terms of mean accuracy, as shown in Fig. 8 and Table 2. Notice that during epochs 211 to 231 as the shaded area in Fig. 8, the LOS classification recall is significantly degraded. The shadow matching scoring heatmap with the  $C/N_0$ -based and grid-based classification results are shown in Fig. 9 during this period. The vehicle is in a narrow street with tall buildings on both sides, receiving a limited number of LOS satellites and

most of the received signals are very weak. Only 2 of the 22 satellites in the ephemeris are classified to be LOS with a probability of over 50% by the  $C/N_0$  model. As a result, the shadow matching mistakenly gives a higher score to the incorrect candidate position, making both solution-based and grid-based methods badly performed. As shown by the sky-plot in Fig. 9, it is a very difficult scenario for GNSS that over 67% of the sky is blocked by the buildings. Without enough satellites, the GNSS receiver failed to provide a positioning solution. Although the LOS classification recall is degraded by incorrect shadow matching solutions, the NLOS classification

recalls of the proposed methods are still accurate, maintaining the overall accuracy around 80% during this period. As the metric taking both precision and recall into account, the F1 scores of both solution-based method and grid-based method are over 10% higher than that of the  $C/N_0$ -based method. Therefore, the proposed methods can achieve better satellite visibility estimation performance in the urban scenario, especially for the NLOS classification.

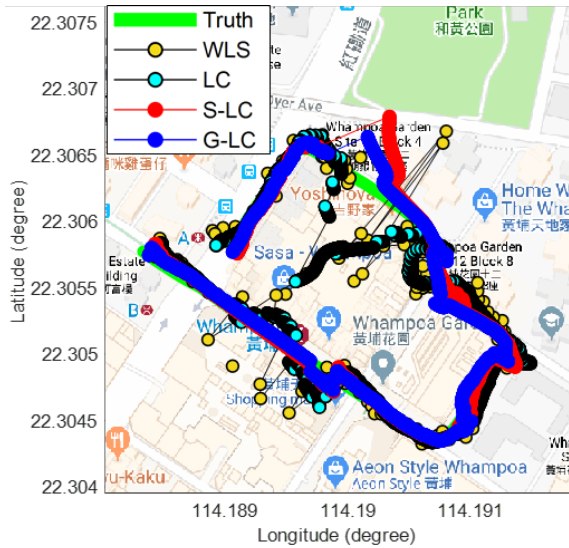


Fig. 10. Positioning results of weighted least squares (WLS) method, conventional loosely-coupled GNSS/INS integration method (LC), the shadow matching solution-based satellite visibility aided loosely-coupled method (S-LC) and the grid-based satellite visibility aided loosely-coupled method (G-LC) and the vehicle’s ground truth (Truth).

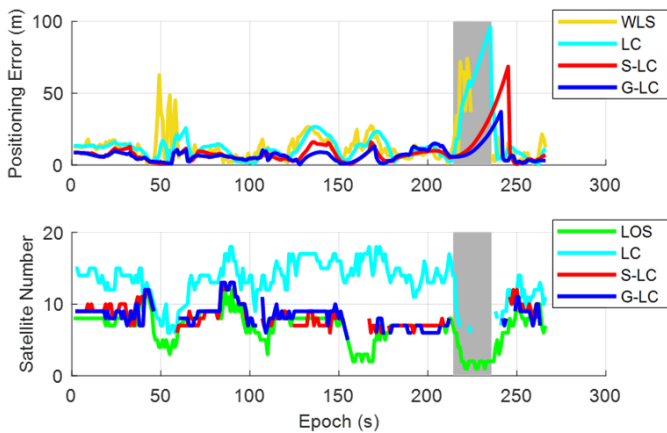


Fig. 11. The positioning error and corresponding in-use satellite number for different loosely-coupled integration methods. The green line indicates the total truly-LOS satellite number. The line is empty if the measurement amount is insufficient to provide a positioning solution. The shaded area denotes the GNSS-limited period during the experiment.

Aided by the satellite visibility estimation, the proposed loosely-coupled GNSS/INS integrated positioning result is shown in Fig. 10 and Fig. 11. The positioning root mean squares error (RMSE), the ratio of the epochs that the positioning solution is available for the corresponding method (availability) are shown in Table 3 with different methods. The GNSS WLS performance is severely degraded by NLOS receptions, resulting in a positioning error of 22.6 meters in RMSE. At

some epochs, the positioning error exceeds 50 meters. Due to insufficient satellites, it even fails to provide solutions during the GNSS-limited area. By integrating the INS, the LC guarantees full availability of solutions and is more robust against GNSS enormous errors. However, with regards to the true satellite visibility, more than half of the measurements used for positioning are NLOS measurements, contributing overall 21.6 meters RMSE. Moreover, during the GNSS-limited period, the INS error is severely accumulated. Aided by the solution-based visibility, the S-LC mitigates the NLOS measurements before the integration. Although only 78.4% of the epochs have enough GNSS measurements for integration after NLOS exclusion, the measurements for integration are guaranteed to be accurate, decreasing the position RMSE to 13.4 meters. Since the preceding grid-based method is more robust on NLOS classification, G-LC further improves the positioning accuracy with an RMSE of only 8.7 meters.

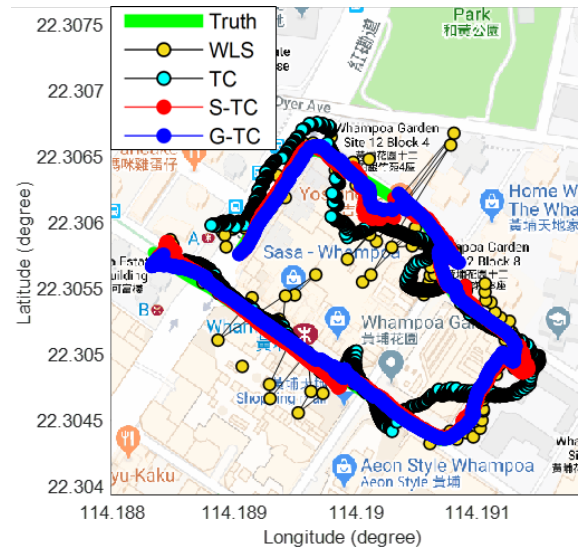


Fig. 12. Positioning results of weighted least squares (WLS) method, conventional tightly-coupled GNSS/INS integration method (TC), the shadow matching solution-based satellite visibility aided tightly-coupling method (S-TC) and the grid-based satellite visibility aided tightly-coupling method (G-TC) and the vehicle’s ground truth (Truth).

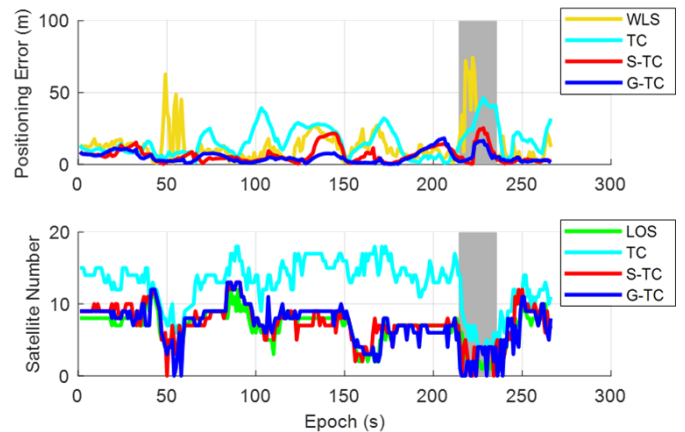


Fig. 13. The positioning error and corresponding in-use satellite number for different tightly-coupled integration methods. The green line indicates the truly-LOS satellite number. The shaded area denotes the GNSS-limited period.

For the tightly-coupled approach, the positioning solution of different GNSS/INS integration methods are shown in Fig. 12, Fig. 13 and Table 3. By integrating the raw GNSS measurements, i.e., pseudorange and pseudorange rate, with INS, the TC achieves a better positioning performance with an RMSE of 18.9 meters, nearly 3 meters improvement over the conventional LC method. Since the integrated measurements still containing NLOS error, the performance of conventional TC method is very limited. By using the shadow matching solution to identify and select the LOS raw measurements for integration, the S-TC greatly reduces the positioning error to 8.5 meters (RMSE). Noted that the integration is bypassed if all the measurements are classified as NLOS from the visibility estimation, resulting in a 97.4% availability for S-TC method.

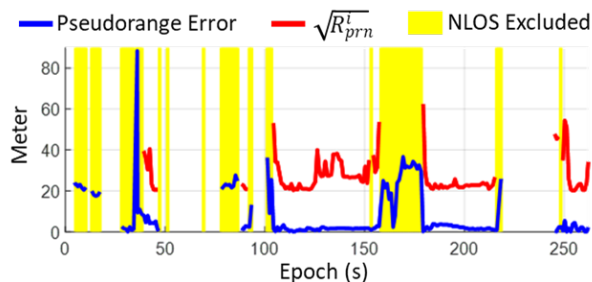


Fig. 14. The pseudorange error and the square root of the measurement noise covariance of the satellite-100 during the G-TC positioning. The yellow area denotes the measurement is classified as NLOS and excluded by the proposed method. The blank area indicates the measurement is not received.

Finally, the proposed G-TC method can use the estimated NLOS probability to adjust the measurement noise covariance, in order to improve the integration performance. The adjusted covariance of the pseudorange measurement from the satellite-100 is shown with a square root form in Fig. 14, and it is compared with the corresponding pseudorange error. The pseudorange error is estimated based on the receiver ground-truth and the reference station information with a double differenced approach [38]. The adjusted covariance has the same trend as the pseudorange error. Especially when the measurement error is increased at epoch 157, the corresponding covariance is adjusted with a higher value. As the error keeps increasing, the measurement is also classified as NLOS and excluded by the proposed method. When the measurement error reduces at epoch 178, the covariance is adjusted back to a smaller value. In summary, the proposed G-TC method can not only exclude NLOS measurements, but also adjust the measurement noise covariance to an appropriate value for sensor integration. As a result, the G-TC achieves the positioning accuracy as 6.5 meters (RMSE), which is the best performance among different methods and nearly three times better than the conventional TC method.

TABLE III

THE RMSE AND AVAILABILITY OF DIFFERENT POSITIONING METHODS DURING THE VEHICULAR EXPERIMENT

Positioning Method	WLS	LC	TC	S-LC	G-LC	S-TC	G-TC
RMSE (m)	22.6	21.6	18.9	13.4	8.7	8.5	6.5
Availability	94.7%	100%	100%	100%	100%	100%	100%

### C. Computational Load Analysis

Since the proposed method conducts shadow matching during the integration, its computational load is analyzed comparing to the conventional method. The analysis is conducted on the MATLAB programming platform of the laptop with Intel(R) Core(TM) i7-7700HQ CPU @ 2.80GHz processor, 16GB RAM. As Fig. 15 shows, although the proposed shadow matching aided GNSS/INS integration methods require an extra 0.03 second comparing to the conventional method. It is noted that the loosely-coupled approach requires a bit more computation due to the GNSS least-squares positioning. The practical engineering issues of implementing shadow matching are discussed in [39], including the computational load.

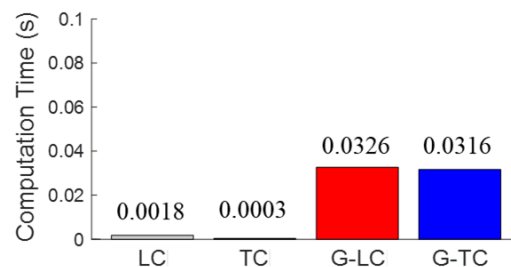


Fig. 15. The computational load of different methods for a single epoch positioning solution.

## VII. CONCLUSIONS

In this study, two satellite visibility estimation methods are developed based on the GNSS shadow matching in the urban scenario. The shadow matching solution-based method uses the shadow matching positioning result to improve the satellite visibility estimation accuracy, especially the NLOS classification accuracy. The shadow matching grid-based method can obtain a similar classification accuracy improvement with better robustness. Both proposed methods improve LOS/NLOS classification accuracy with at least 10% in most of the scenarios in urban areas, compared to the conventional  $C/N_0$ -based method. By using the proposed method to exclude NLOS measurements, the contribution of the 3DMA GNSS shadow matching is extended to further improve the loosely-coupled or tightly-coupled GNSS/INS integrated positioning performance. Using the grid-based satellite visibility information to exclude NLOS measurements and adjusting the measurement noise covariance, the proposed shadow matching aided GNSS/INS integration method achieves an RMSE of 6.5 meters of a vehicular test in the dense urban scenario, which is nearly 3 times more accurate than the conventional tightly-coupled integration approach. The proposed method also shows the potential to further integrate with other sensors (LiDAR, vision) to fulfill the positioning performance requirements for autonomous driving. However, for the harsh environment with limited sky-view, the NLOS-exclusion method may only have a limited amount of measurements for positioning, resulting in the estimation is sensitive to the error and not robust. Therefore, the 3DMA GNSS NLOS-correction method is worth to be studied to guarantee the system robustness in the harsh environment.

## REFERENCES

- [1] J. Mervis, "Not so fast," *Science*, vol. 358, no. 6369, pp. 1370-1374, Dec. 2017.
- [2] B. Paden, M. Čáp, S. Z. Yong, D. Yershov, and E. Frazzoli, "A survey of motion planning and control techniques for self-driving urban vehicles," *IEEE Transactions on Intelligent Vehicles*, vol. 1, no. 1, pp. 33-55, Mar. 2016.
- [3] S. Kamijo, Y. Gu, and L.-T. Hsu, "Autonomous vehicle technologies: Localization and mapping," *IEICE ESS Fundamentals Review*, vol. 9, no. 2, pp. 131-141, Oct. 2015.
- [4] R. Hussain and S. Zeadally, "Autonomous cars: Research results, issues, and future challenges," *IEEE Communications Surveys & Tutorials*, vol. 21, no. 2, pp. 1275-1313, 2019.
- [5] P. D. Groves, *Principles of GNSS, Inertial, and Multisensor Integrated Navigation Systems*. Norwood, MA, USA: Artech House, 2013.
- [6] A. Noureldin, T. B. Karamat, M. D. Eberts, and A. El-Shafie, "Performance enhancement of MEMS-based INS/GPS integration for low-cost navigation applications," *IEEE Transactions on Vehicular Technology*, vol. 58, no. 3, pp. 1077-1096, Mar. 2009.
- [7] H. Liu, S. Nassar, and N. El-Sheimy, "Two-filter smoothing for accurate INS/GPS land-vehicle navigation in urban centers," *IEEE Transactions on Vehicular Technology*, vol. 59, no. 9, pp. 4256-4267, Nov. 2010.
- [8] G. Zhang and L.-T. Hsu, "Intelligent GNSS/INS integrated navigation system for a commercial UAV flight control system," *Aerospace Science and Technology*, vol. 80, pp. 368-380, 2018.
- [9] Z. Wu, M. Yao, H. Ma, W. Jia, and F. Tian, "Low-cost antenna attitude estimation by fusing inertial sensing and two-antenna GPS for vehicle-mounted satcom-on-the-move," *IEEE Transactions on Vehicular Technology*, vol. 62, no. 3, pp. 1084-1096, Mar. 2013.
- [10] T. Takasu and A. Yasuda, "Development of the low-cost RTK-GPS receiver with an open source program package RTKLIB," in *International Symposium on GPS/GNSS*, 2009, pp. 4-6.
- [11] R. W. Wolcott and R. M. Eustice, "Visual localization within lidar maps for automated urban driving," in *IEEE/RSJ International Conference on Intelligent Robots and Systems*, 2014, pp. 176-183.
- [12] B. Ranft and C. Stiller, "The role of machine vision for intelligent vehicles," *IEEE Transactions on Intelligent Vehicles*, vol. 1, no. 1, pp. 8-19, Mar. 2016.
- [13] J. Zhang and S. Singh, "LOAM: Lidar odometry and mapping in real-time," in *Proceedings of Robotics: Science and Systems Conference*, 2014, vol. 2, p. 9.
- [14] G. Bresson, Z. Alsayed, L. Yu, and S. Glaser, "Simultaneous localization and mapping: A survey of current trends in autonomous driving," *IEEE Transactions on Intelligent Vehicles*, vol. 2, no. 3, pp. 194-220, Sep. 2017.
- [15] N. Zhu, J. Marais, D. Bétaille, and M. Berbineau, "GNSS position integrity in urban environments: A review of literature," *IEEE Transactions on Intelligent Transportation Systems*, vol. 19, no. 9, pp. 2762-2778, Sep. 2018.
- [16] P. D. Groves, "Multipath vs. NLOS signals," *Inside GNSS*, vol. 8, no. 6, pp. 40-42, 2013.
- [17] G. Zhang and L.-T. Hsu, "A new path planning algorithm using a GNSS localization error map for UAVs in an urban area," *Journal of Intelligent & Robotic Systems*, vol. 94, no. 1, pp. 219-235, Apr. 2019.
- [18] E. Realini and M. Reguzzoni, "goGPS: Open source software for enhancing the accuracy of low-cost receivers by single-frequency relative kinematic positioning," *Measurement Science and Technology*, vol. 24, no. 11, p. 115010, 2013.
- [19] L.-T. Hsu, H. Tokura, N. Kubo, Y. Gu, and S. Kamijo, "Multiple faulty GNSS measurement exclusion based on consistency check in urban canyons," *IEEE Sensors Journal*, vol. 17, no. 6, pp. 1909-1917, Mar. 2017.
- [20] P. D. Groves and Z. Jiang, "Height aiding, C/N0 weighting and consistency checking for GNSS NLOS and multipath mitigation in urban areas," *Journal of Navigation*, vol. 66, no. 5, pp. 653-669, Sep. 2013.
- [21] R. Sun, L.-T. Hsu, D. Xue, G. Zhang, and W. Y. Ochieng, "GPS signal reception classification using adaptive neuro-fuzzy inference system," *Journal of Navigation*, vol. 72, no. 3, pp. 685-701, May. 2019.
- [22] J. K. Ray, M. E. Cannon, and P. Fenton, "GPS code and carrier multipath mitigation using a multiantenna system," *IEEE Transactions on Aerospace and Electronic Systems*, vol. 37, no. 1, pp. 183-195, Jan. 2001.
- [23] L. Wang, P. D. Groves, and M. K. Ziebart, "GNSS shadow matching: Improving urban positioning accuracy using a 3D city model with optimized visibility scoring scheme," *Navigation: Journal of the Institute of Navigation*, vol. 60, no. 3, pp. 195-207, 2013.
- [24] P. D. Groves, "Shadow matching: A new GNSS positioning technique for urban canyons," *Journal of Navigation*, vol. 64, no. 3, pp. 417-430, Jul. 2011.
- [25] P. D. Groves and M. Adjrard, "Likelihood-based GNSS positioning using LOS/NLOS predictions from 3D mapping and pseudoranges," *GPS Solutions*, vol. 21, no. 4, pp. 1805-1816, Oct. 2017.
- [26] P. D. Groves and M. Adjrard, "Performance assessment of 3D-mapping-aided GNSS part 1: Algorithms, user equipment, and review," *Navigation: Journal of the Institute of Navigation*, vol. 66, no. 2, pp. 341-362, 2019.
- [27] M. Obst, S. Bauer, and G. Wanielik, "Urban multipath detection and mitigation with dynamic 3D maps for reliable land vehicle localization," in *Proceedings of the 2012 IEEE/ION Position, Location and Navigation Symposium*, 2012, pp. 685-691.
- [28] L.-T. Hsu, Y. Gu, and S. Kamijo, "3D building model-based pedestrian positioning method using GPS/GLONASS/QZSS and its reliability calculation," *GPS Solutions*, vol. 20, no. 3, pp. 413-428, Jul. 2016.
- [29] T. Suzuki and N. Kubo, "Correcting GNSS multipath errors using a 3D surface model and particle filter," in *Proceedings of the 26th International Technical Meeting of The Satellite Division of the Institute of Navigation (ION GNSS+ 2013)*, 2013, pp. 1583-1595.
- [30] S. Miura, L.-T. Hsu, F. Chen, and S. Kamijo, "GPS error correction with pseudorange evaluation using three-dimensional maps," *IEEE Transactions on Intelligent Transportation Systems*, vol. 16, no. 6, pp. 3104-3115, Dec. 2015.
- [31] N. I. Ziedan, "Urban positioning accuracy enhancement utilizing 3D buildings model and accelerated ray tracing algorithm," in *Proceedings of the 30th International Technical Meeting of The Satellite Division of the Institute of Navigation (ION GNSS+ 2017)*, Portland, OR, USA, 2017, pp. 3253-3268.
- [32] H. F. Ng, G. Zhang, and L.-T. Hsu, "Range-based 3D mapping aided GNSS with NLOS correction based on skyplot with building boundaries," in *Proceedings of the ION 2019 Pacific PNT Meeting*, Honolulu, HI, USA, 2019, pp. 737-751.
- [33] Y. Gu, L. Hsu, and S. Kamijo, "GNSS/onboard inertial sensor integration with the aid of 3-D building map for lane-level vehicle self-localization in urban canyon," *IEEE Transactions on Vehicular Technology*, vol. 65, no. 6, pp. 4274-4287, Jun. 2016.
- [34] P. D. Groves and M. Adjrard, "Multi-epoch 3D mapping aided GNSS using a grid filter," in *Proceedings of the 31st International Technical Meeting of The Satellite Division of the Institute of Navigation (ION GNSS+ 2018)*, Miami, FL, USA, 2018, pp. 3335-3356.
- [35] P. D. Groves, L. Wang, and M. Ziebart, "Shadow matching: Improved GNSS accuracy in urban canyons," *GPS World*, vol. 23, no. 2, pp. 14-18, Feb. 2012.
- [36] E. Kaplan and C. Hegarty, *Understanding GPS: Principles and Applications*. Norwood, MA, USA: Artech House, 2005.
- [37] H. Gao and P. D. Groves, "Context determination for adaptive navigation using multiple sensors on a smartphone," in *Proceedings of the 29th International Technical Meeting of the Satellite Division of The Institute of Navigation (ION GNSS+ 2016)*, Portland, OR, 2016, pp. 742-756.
- [38] B. Xu, Q. Jia, Y. Luo, and L.-T. Hsu, "Intelligent GPS L1 LOS/multipath/NLOS classifiers based on correlator-, RINEX- and NMEA-level measurements," *Remote Sensing*, vol. 11, no. 16, p. 1851, 2019.
- [39] P. D. Groves, L. Wang, M. Adjrard, and C. Ellul, "GNSS shadow matching: The challenges ahead," in *Proceedings of the 28th International Technical Meeting of The Satellite Division of the Institute of Navigation (ION GNSS+ 2015)*, Tampa, FL, 2015, pp. 2421-2443.



**Guohao Zhang** received the bachelor's degree in mechanical engineering and automation from University of Science and Technology Beijing, China, in 2015. He received the master's degree in Mechanical Engineering and currently pursuing the Ph.D. degree in the Interdisciplinary Division of Aeronautical and Aviation

Engineering, the Hong Kong Polytechnic University. His research interests including GNSS urban localization, cooperative positioning and multi-sensor integrated navigation.



**Weisong Wen** was born in Ganzhou, Jiangxi, China. He is a Ph.D. candidate in mechanical engineering, the Hong Kong Polytechnic University. His research interests include multi-sensor integrated localization for autonomous vehicles, SLAM and GNSS positioning. He was a visiting student researcher in University of

California, Berkeley (UCB) in 2018.



**Bing Xu** is currently a Postdoctoral Fellow with Interdisciplinary Division of Aeronautical and Aviation Engineering, The Hong Kong Polytechnic University. He received his B.S. and Ph.D. degrees in Network Engineering and Navigation Guidance and Control from Nanjing University of Science and Technology, China, in 2012 and 2018, respectively. His

research focuses on signal processing in software-defined GNSS receivers.



**Li-Ta Hsu (S'09–M'15)** received the B.S. and Ph.D. degrees in aeronautics and astronautics from National Cheng Kung University, Taiwan, in 2007 and 2013, respectively. He is currently an assistant professor with the Division of Aeronautical and Aviation Engineering, Hong Kong Polytechnic University, before

he served as post-doctoral researcher in Institute of Industrial Science at University of Tokyo, Japan. In 2012, he was a visiting scholar in University College London, U.K. He is an Associate Fellow of RIN. His research interests include GNSS positioning in challenging environments and localization for pedestrian, autonomous driving vehicle and unmanned aerial vehicle.